CrossMark

RESEARCH PAPER

Uncoupled dual hardening model for clays considering the effect of overconsolidation and intermediate principal stress

Amit Prashant · Dayakar Penumadu

Abstract A constitutive model is proposed for clays based on the experimental observations from a series of flexible boundary true triaxial shear tests on cubical specimens of light to heavily overconsolidated kaolin clay. The proposed model adequately captures the combined effect of overconsolidation and intermediate principal stress. Overconsolidated clays often exhibit nonlinear stress–strain response at much lower stress levels than what is predicted by the existing constitutive theories/models. Experimental results for kaolin clay demonstrated sudden failure response before reaching the critical state, which became more prominent for higher relative magnitudes of intermediate principal stress. The observed stress state at failure is governed by the third invariant of stress tensor and the pre-failure yielding of the material by the second invariant of deviatoric stress tensor. The proposed constitutive model considers these issues with a few simplifying assumptions. The assumed yield surface has a droplet shape in q–p' stress space with hardening based on both plastic volumetric and shear deformations. A dynamic failure criterion is employed in the current formulation that grows in size as a function of consolidation history. Pre-failure yielding is governed by a reference surface, which is different from the failure surface.

Keywords Clays · Constitutive model · Failure criteria · Overconsolidated · Strain hardening · Sudden failure response · Yield surface

List of symbols

b	Intermediate principal stress ratio
C_f	Failure surface parameters
F_p, F_q	Total plastic flow equivalent for volumetric strain, shear strain
I_3, I_{3f}	Third invariant of stress tensor, at failure
n_f	Hardening parameter
n_g	Plastic potential parameter
H	Plastic hardening modulus
h_q	Shear hardening factor
OCR	Overconsolidation ratio
p'	Mean effective stress
p_o'	Pre-consolidation pressure
q, q_f	Deviatoric stress in invariant form, at failure
$\Delta u, \Delta u_f$	Excess pore-pressure, at failure
v	Specific volume (1 + void ratio)
x, y	Cartesian coordinates on octahedral plane
v	Poisson's ratio
κ	Slope of unloading–reloading line [in $v - \log(p')$ plane]
λ	Slope of virgin consolidation line [in $v - \log(p')$ plane]
ξ	Shear stress mapping function
ψ	Asymptoting factor for failure
ε_{ij}	Strain state
σ_{ij}'	Effective stress state
$\sigma_1, \sigma_2, \sigma_3$	Major, intermediate and minor principal stress

A. Prashant
Civil Engineering, Indian Institute of Technology Gandhinagar, Gujarat, India
e-mail: ap@iitgn.ac.in

D. Penumadu (✉)
Department of Civil and Environmental Engineering, University of Tennessee, Knoxville, TN, USA
e-mail: dpenumad@utk.edu

1 Introduction

Engineering applications demand material constitutive models with the virtue of simple formulation, minimum number of parameters, simple experiments for calibration and some physical meaning of the state variables. Over the last few decades, several constitutive theories related to soils have been formulated considering different aspects of the observed soil behavior [4, 6, 14, 15, 20, 29, 31, 39]. These studies recognize that soils show highly nonlinear stress–strain response and the nonlinearity begins at small strains itself [8]. The past history of both volumetric and distortional deformations leaves their impression in the memory of clay and governs the behavior when the material is subjected to further loading [1, 16, 17, 43]. In many cases, clay specimens during laboratory testing show sudden failure before reaching the critical state. Onset of instability within deforming specimen during shear test could be a possible reason for such premature failure [22, 35, 37]. The stress-induced anisotropy is another aspect, which has significant influence on the soil's shear behavior.

Prashant and Penumadu [26, 27] performed a series of true triaxial tests on cubical specimens of lightly to heavily overconsolidated kaolin clay and quantified the effects of intermediate principal stress and overconsolidation on the shear stress–strain behavior of clay. The cubical clay specimens were prepared through one-dimensional consolidation of kaolin clay slurry at 207 kPa in a plexi-glass consolidometer as described by Penumadu et al. [24]. In the current paper, the authors propose a constitutive model for clays with due consideration to the earlier findings of their experimental study on kaolin clay and by addressing most of the experimental observations related to effects of overconsolidation and true triaxial state of stress. The formulation is based on the well-defined and widely accepted concept of the elasto-plasticity theory. The proposed model considers a balance between the simplicity of formulation and accuracy of results to predict response of clay-type geomaterials as continuum. It is assumed that the loading is monotonic and that large stress reversals including sudden directional changes in stress path are not involved. Temperature and time effects are assumed to be absent.

Basic concept of the proposed model has been developed over the assumptions of Cam-clay elasto-plasticity [30]. The volumetric hardening employed in Cam-clay plasticity has been also used in the current model as a part of the hardening rule along with an uncoupled shear hardening of clay [36]. A non-associative flow rule (different yield and plastic potential functions) is used to describe the clay behavior, which is considered more appropriate choice for geomaterials [9, 14, 21, 23]. The model proposed in this paper has two components. The first component considers the behavior of normally consolidated (NC) and overconsolidated (OC) clay in triaxial compression plane. The issues related to highly nonlinear stress–strain relationship for OC clay soil, sudden failure response and dual hardening are addressed in this part of the formulation. The second component incorporates the effect of intermediate principal stress by defining the failure surface as a function of third invariant of stress tensor in the octahedral plane.

The proposed model requires merely two standard laboratory tests (consolidation test and triaxial compression test) to determine all the six parameters involved with its calibration. The procedure of model calibration has been demonstrated by using the data for kaolin clay. The ability to precisely capture the complex mechanical behavior of clay soil using the proposed model has been illustrated by evaluating its predictions with the experimental data based on a series of true triaxial undrained shear tests on kaolin clay.

In summary, the contributions of this paper relate to the development of a constitutive model for clays subjected to generalized loading based on the observations from an extensive experimental study using a flexible boundary true triaxial testing system. The model incorporates several complex issues related to clay behavior such as deviatoric hardening, combined effect of intermediate principal stress and overconsolidation on nonlinear stress–strain response, shear strength with sudden failure response and dilative/contractive behavior of clay during shearing.

2 Framework of the proposed model in triaxial compression plane

The model formulation in q–p' space is discussed in this section, where q is deviatoric stress and p' is mean effective stress. The corresponding shear and volumetric strains are denoted by $d\varepsilon_q$ and $d\varepsilon_p$. These terms can be defined as functions of the effective stress state σ_{ij}' and the strain state ε_{ij}, as shown in Eqs. (1) and (2).

$$p' = \frac{\sigma_{ii}'}{3}; \quad q = \sqrt{\frac{3}{2} s_{ij} s_{ij}}; \quad \text{where } s_{ij} = \sigma_{ij}' - \frac{\sigma_{kk}'}{3} \delta_{ij} \quad (1)$$

$$\varepsilon_p = \varepsilon_{ii}; \quad \varepsilon_q = \sqrt{\frac{2}{3} e_{ij}' e_{ij}'}; \quad \text{where } e_{ij}' = \varepsilon_{ij} - \frac{\varepsilon_{kk}}{3} \delta_{ij} \quad (2)$$

Here, Kronecker delta $\delta_{ij} = 1$ for $i = j$, and $\delta_{ij} = 0$ for $i \neq j$.

2.1 Modeling elastic behavior

The proposed model adopts pressure-dependent elasticity of Cam-clay theory [32]. Although this elastic model does

not confirm to conservation of energy [44], it is considered here for merely its simplicity and for the fact that it is applied in many other popular models. This model considers elastic components of the volumetric and shear deformations to be uncoupled from each other and independently relates to the changes in p' and q, respectively. It requires two elastic parameters, slope of the unload–reload curve in $v - \ln(p')$ space during isotropic compression κ and the Poisson's ratio v. Here, $v (= 1 + \text{void ratio})$ is known as specific volume of soil. The Young's modulus E' is defined in Eq. (3), which provides the relationship between incremental elastic strain $d\varepsilon_{ij}^e$ and stress $d\sigma_{ij}$ given in Eq. (4).

$$E' = \frac{3(1-2v)vp'}{\kappa} \tag{3}$$

$$d\varepsilon_{ij}^e = \frac{\kappa}{3(1-2v)vp'}\left[(1+v)d\sigma_{ij} - v\delta_{ij}d\sigma_{kk}\right] \tag{4}$$

2.2 Yield surface

In the elasto-plasticity theory, normally consolidated clay is assumed to have its stress state on the yield surface and that it experiences plastic deformations with growing yield surface when subjected to further loading. Overconsolidated stress state remains inside the yield surface and any change in stress state causes purely elastic deformation unless the new stress state reaches a point on the initial yield surface. Using the data from a series of true triaxial tests on kaolin clay, Prashant and Penumadu [27] reported shape and size of the initial yield surface in $q-p'$ space. The proposed expression looked similar to the equation of yield surface in original Cam-clay model [31], but it was different in terms of its shape in $q-p'$ space. The teardrop shape of yield surface had its end point at $p' = 0$ instead of that at the pre-consolidation stress in original Cam-clay model. It is in fact similar to the one suggested by Lade [13] based on the plastic work contour calculations. Sultan et al. [33] also observed similar shape of yield surface for Boom clay. The present model assumes similar shape of the yield surface which is described using the yield function f given by Eq. (5).

$$f = \left(\frac{q}{q_o}\right)^2 + \left(\frac{p'}{p_o'}\right)^2 \ln\left(\frac{p'}{p_o'}\right) = 0 \tag{5}$$

Here, p_o' is pre-consolidation pressure representing isotropic consolidation history of clay, and q_o is another state variable defining the size of yield surface along deviatoric stress axis, which captures the shearing history of clay. Hence, the variable p_o' accounts for the volumetric component, and q_o represents the distortional counterpart of the permanent deformation history of a soil mass. Both p_o' and q_o together define the hardening behavior of clay

and, in essence, reflect the present state of the soil structure. The variable q_o plays a role in this model along the lines of kinematic hardening often used in some of the earlier models [3, 5, 21, 29, 34]. However, in the present model, q_o has been kept uncoupled from p_o' to keep the formulation simple, and the yield surface always remains symmetric about the hydrostatic axis. Figure 1 illustrates growth of the yield surface with change in the values of hardening variables p_o' and q_o. Figure 1a shows the yield surface for three values of $p_o' = 150$, 200 and 250 kPa and constant q_o at 300 kPa, and Fig. 1b shows it for three values of $q_o = 150$, 200 and 250 kPa by keeping
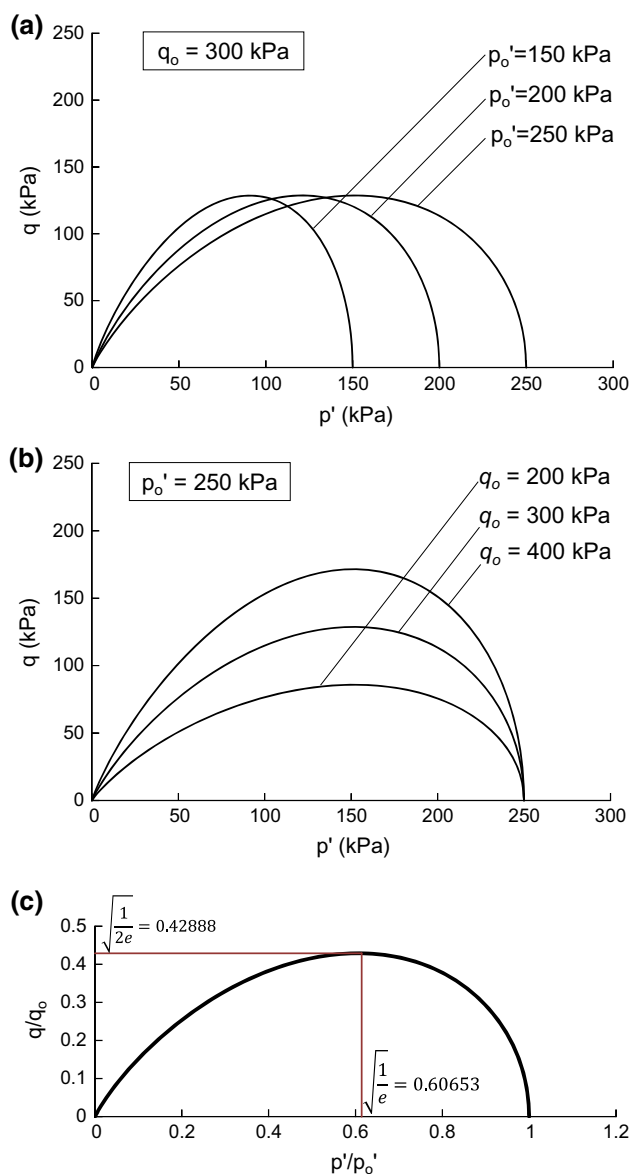

Fig. 1 Shape of yield surface in $q-p'$ stress space, **a** growth of yield surface with change in consolidation history p_o', and **b** growth of yield surface with change in state variable q_o, **c** normalized yield surface

p_o' constant at 250 kPa. These surfaces are self-similar, and their sizes have linear relationship with p_o' and q_o. Therefore, the yield surface can be, in fact, normalized by p_o' and q_o along the respective axes, which brings out a constant yield surface in the normalized stress space shown in Fig. 1c. The deviatoric peak of the yield surface occurs at $p'/p_o' = \sqrt{1/e} = 0.60653$ and $q/q_o = \sqrt{1/(2e)} = 0.42888$. Similar to how the past literature treated the variable p_o', this study introduces a deviatoric peak value on yield surface using the variable q_o. In the proposed model, the variable q_o is a constant multiple ($\approx 1/ 0.42888 = 2.332$ times) of the peak deviatoric stress on yield surface. One can alternatively define q_o to be same as the peak deviatoric stress on yield surface. In that case, a constant term ($\approx 2.332^2 = 5.437$) will be multiplied in the second term of the yield function to satisfy the equation. However, such a change adds no value to the formation after calibration of initial value of q_o. Hence, the yield function is kept simple in the proposed model although q_o is a constant multiple of the peak deviatoric stress on yield surface.

2.3 Failure surface

Mayne [18], and Mayne and Swanson [19] summarized the undrained shear strength of different clays reported in literature. They showed that the normalized strength (S_u/σ_{vo}') is a function of overconsolidation ratio (OCR) for most of the clays, which was originally identified by Ladd and Foott [10]. Further, Roscoe et al. [31] suggested that the shear strength is uniquely related to void ratio and that, at any stress state, the void ratio can be represented using the mean effective stress, pre-consolidation stress and the compressibility parameters of soil. Based on the above findings, one can easily derive an expression of failure surface in q–p' space as a function of pre-consolidation pressure [27], which implicitly incorporates the effect of void ratio. The model developed in the present study uses a similar failure surface in triaxial plane (represented by q–p' space), which describes deviatoric stress at failure q_f by Eq. (6).

$$q_f = C_f p' \left(\frac{p_o'}{p'}\right)^{\Lambda_o} \tag{6}$$

Two scalar parameters C_f and Λ_o are used to define the failure surface, which depend only on the type of clay soil. The parameter Λ_o ($= 1 - \kappa/\lambda$) essentially depends on the slopes of unload–reload line κ and normal consolidation line λ in $v - \ln(p')$ space during isotropic compression. Figure 2 shows the shape and size of a typical failure surface in comparison with a typical initial yield surface. It is worth noticing here that the failure surface is a function of pre-consolidation pressure p_o', and it grows linearly in
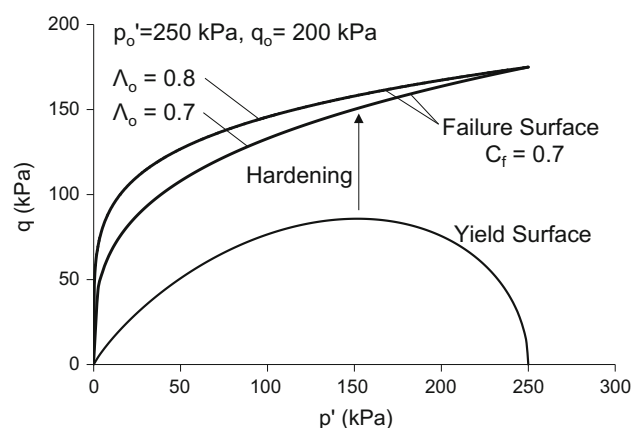

Fig. 2 Typical shapes of yield and failure surfaces in q–p' stress space, plots for $p_o' = 250$ kPa and $q_o = 200$ kPa
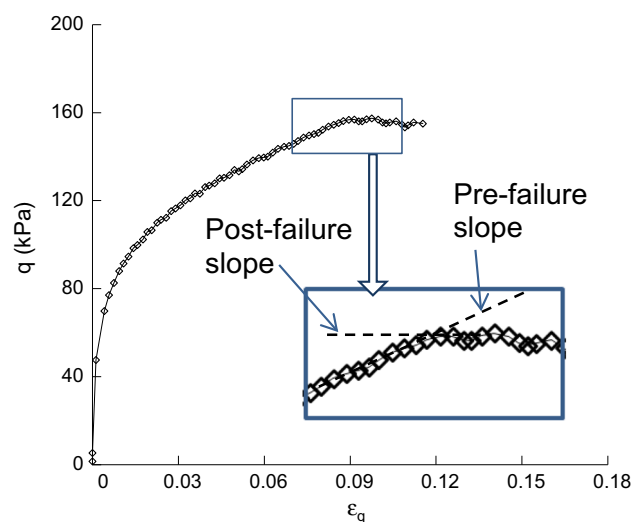

Fig. 3 Shear stress–strain relationship with sudden failure response (undrained true triaxial shearing of NC clay specimen for $b = 1$)

size with increase in p_o' value and terminates at p_o' along the p' axis. This assumption may not hold true for an extremely large stress range as indicated in [2].

The Modified Cam-Clay (MCC) model [30] assumes critical state at the mean stress ratio $p'/p_o' = 2$, at which the shear stress ratio q/p' is defined by a soil parameter M. If the failure surface of Eq. (6) is correlated with the MCC model, the parameters M and C_f will have a constant relationship as $M = 2^{\Lambda_o} C_f$. The current failure surface has an advantage over the MCC model since it provides freedom for defining p'/p_o' ratio at failure as a soil property instead of a fixed scalar value for all soil types. This flexibility employed in our model facilitates better predictions of pore-pressure or volumetric strains during shearing.

Prashant and Penumadu [27, 28] observed that the kaolin clay specimens experienced an abrupt loss of the shear

stiffness at failure and showed sudden failure during flexible boundary true triaxial tests on remolded cubical specimens in undrained conditions (Fig. 3). The severity of the sudden failure response varied with OCR of the specimen. While it was relatively less significant for the case of NC clay, the OC specimens exhibited prominent sudden failure response at much lower shear strains. This response was also found to depend on the relative magnitude of intermediate principal stress. The failure stress state for various stress paths could be represented using a failure criteria based on the third invariant of stress tensor I_3 ($=\sigma_{11} \cdot \sigma_{22} \cdot \sigma_{33}$) in the octahedral plane as shown in Fig. 4, and it was applicable for all the cases of OCR values. Wang and Lade [38] also reported similar observations related to the failure stress state based on drained tests on Santa Monica beach sand. The I_3-based failure criteria have been also used in several other models in the past [11–13, 41]. Considering the shape of failure surface in both triaxial plane (Eq. 6) and octahedral plane, the following expression defines the complete failure criteria in the present model.

$$I_{3\mathrm{f}} = \left\langle \frac{2}{27}q_{\mathrm{f}}^3 - \frac{1}{3}q_{\mathrm{f}}^2 p' + p'^3 \right\rangle \tag{7}$$

where $\langle \rangle$ are Macaulay brackets. They constrain the failure surface to exist only in the positive quadrant of three-dimensional stress space, by which it is considered that the frictional material will fail if one of the acting principal stresses goes to zero [42]. This condition is based on a widely accepted assumption of no cohesion in frictional materials. Hence, the stable state of material (stress state before failure condition) in three-dimensional stress space will exist for $I_3 > I_{3\mathrm{f}}$.
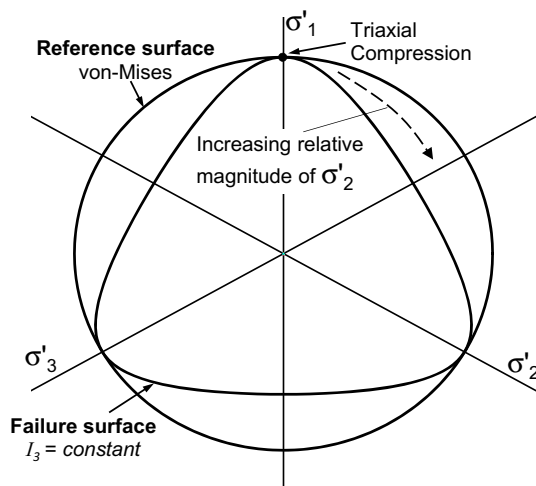

Fig. 4 Typical shapes of reference and failure surfaces in octahedral plane

2.4 Hardening rule

Plastic hardening (growth) of the yield surface is defined using two state variables p_{o}' and q_{o}, as mentioned earlier in Eq. (5). Similar to Cam-clay plasticity, the pre-consolidation pressure p_{o}' is defined as a function of plastic volumetric strain $\varepsilon_p^{\mathrm{p}}$ and it is independent of plastic shear strains $\varepsilon_q^{\mathrm{p}}$. On the contrary, the state variable q_{o} is defined as a function of only $\varepsilon_q^{\mathrm{p}}$. Hence, the model considers uncoupled hardening of material with respect to volumetric and deviatoric components. In the mathematical form, the hardening rule is given by Eqs. (8) and (9).

$$\frac{\partial p_o'}{\partial \varepsilon_p^{\mathrm{p}}} = \frac{vp_o'}{(\lambda - \kappa)} \qquad \frac{\partial p_o'}{\partial \varepsilon_q^{\mathrm{p}}} = 0 \tag{8}$$

$$\frac{\partial q_o}{\partial \varepsilon_p^{\mathrm{p}}} = 0 \qquad \frac{\partial q_o}{\partial \varepsilon_q^{\mathrm{p}}} = n_f(1 - \xi)\frac{p_o'^2}{p_o' + q_o}\psi \tag{9}$$

Here, n_{f} is a soil constant, ξ a stress state mapping function Ref. [4, 39] and ψ an asymptoting factor against failure criteria. The deviatoric hardening parameter n_{f} of a material defines the rate at which its yield surface will grow in deviatoric direction with increase in q_{o} when subjected to plastic shear deformations. It assumes that when a material undergoes pure shear without change in volume or mean effective stress, it may still experience hardening against distortional deformations and the material structure may preserve the memory of shear stress as long as the loading is monotonic. Such a constant p' test with no significant plastic volumetric response can be easily observed during undrained shearing of lightly OC clay with OCR = 2–2.5, which shows a significant range of hardening in stress space after initial elastic deformations. Although such a test is ideal for calibration of deviatoric hardening parameter, it can be also easily calibrated using data from any other test by following the assumption of uncoupled hardening.

The experimental findings from true triaxial tests on Kaolin clay indicated that the pre-failure stress–strain response was almost independent of failure stress state and it had only marginal influence of intermediate principal stress. A new bounding surface is hypothesized, which is likely to be reached by the stress state in absence of sudden failure response shown by the experiments. At such a (hypothetical) surface, the shear stiffness (tangent modulus) will reach a value of zero prior to large plastic flow. Hence, it can be appropriately assumed that the pre-failure stress–strain behavior is primarily mapped to a reference surface which is of von-Mises type in octahedral plane and follows Eq. (6) in triaxial compression plane. Typical shapes of the reference surface and failure surface are shown in Fig. 4. These two surfaces share a common point at the triaxial compression state ($\sigma_2' = \sigma_3'$), and the gap between them increases as the relative magnitude of

intermediate principal stress increases toward the condition of $\sigma_2' = \sigma_1'$. As shown in Eq. (10), ξ is defined as ratio of the shear stress at current stress state and the shear stress q_f on reference surface (Eq. 6) for the same p' value.

$$\xi = \frac{q}{q_f} \tag{10}$$

The value of ξ ranges from $\xi = 0$ at p'-axis to $\xi = 1$ for $q = q_f$. Therefore, the state variable q_o has strongest relationship with plastic shear strains at p'-axis. However, close to p'-axis, the developed plastic shear strains are relatively too small to cause any significant change in q_o. The relationship goes weaker as the stress state moves away from p'-axis toward the reference surface, and eventually, q_o becomes constant when $q = q_f$.

The asymptoting factor ψ given in Eq. (11) has been used in both hardening rule and plastic potential (in next section).

$$\psi = 1 - \left(\frac{p'^3 - I_3}{p'^3 - I_{3f}}\right)^n \tag{11}$$

This factor is used to predict rapid increase in shear deformations as the I_3 value of stress state reaches close to a specific value of I_{3f} (Eq. 7) according to failure criteria. Hence, the value of exponent in Eq. (11) is chosen to be a high value, such as $n = 10$, so that the stress–strain response remains independent of I_3 unless the stress state is in the proximity of I_{3f} where the sudden failure occurs with large shear deformations. By the use of factor ψ, the stress state never exceeds an I_3-based surface in octahedral plane and follows Eq. (6) in triaxial compression plane. As the stress state reaches at the failure surface of Eq. (7), the value of q_o becomes constant due to the value of ψ going to zero. Both the $\psi = 0$ and $q = q_f$ conditions are achieved simultaneously in triaxial compression case. For all the other cases of intermediate principal stress, $\psi = 0$ condition is achieved before the $q = q_f$ and the hardening of yield surface along q-axis is stopped short at the failure surface before reaching reference surface.

2.5 Plastic potential function

The plastic potential function is used to define the direction of plastic strain increments at any stress state of the material. Based on the experimental findings, it is assumed that the material follows a non-associative flow rule with the plastic potential function defined by Eqs. (12) and (13).

$$g = n_g \left(\frac{q q_o}{p_o'}\right)^2 + p' p_o' \left(\frac{p'}{p_o'}\right)^R \ln\left(\frac{p'}{p_o'}\right) \tag{12}$$

$$R = \left(1 - \Lambda_o^2\right)\left(\frac{q_o}{p_o'}\right)^2 \tag{13}$$

Here, n_g is a soil constant. Figure 5 shows typical shape of the plastic potential function in q–p' space. The strain increment vectors are uniquely defined everywhere on the plastic potential except at $p' = 0$ where the material becomes unstable. A higher value of p' corresponding to the peak of plastic potential signifies that the normally consolidated material will behave relatively less contractive when subjected to shearing. A lower value of the variable Λ_o suggests relatively lesser plastic volume change in comparison with its elastic counterpart, and it is reflected in the plastic potential as well. Similarly, as the value of q_o/p_o' increases during shearing, the peak shifts toward higher values of p' and the material becomes less contractive or more dilative. The derivatives of plastic potential with respect to p' and q are given in Eq. (14). The factor ψ has been multiplied to the p' derivative of the plastic potential to simulate sudden increase in the shear deformations as the stress state approaches the failure surface.

$$\frac{\partial g}{\partial p'} = \psi p'^R p_o'^{1-R}\left(1 - (R+1)\ln\left(\frac{p_o'}{p'}\right)\right) \quad \text{and}$$
$$\frac{\partial g}{\partial q} = n_g(2q)\left(\frac{q_o}{p_o'}\right)^2 \tag{14}$$

The experimental observations of Prashant and Penumadu [27] suggested that the plastic strain increment vector(s) at failure condition had normality to a circular shape of plastic potential in octahedral plane. Thus, the plastic potential defined in Eq. (12) is valid for any proportion of principal stresses. Hence, the model assumes circular plastic potential in octahedral plane (von-Mises type) at all stress states to keep the model simple.

2.6 Incremental stress–strain formulation

During elasto-plastic deformation, the yield surface grows in size by following the hardening rule and the stress state
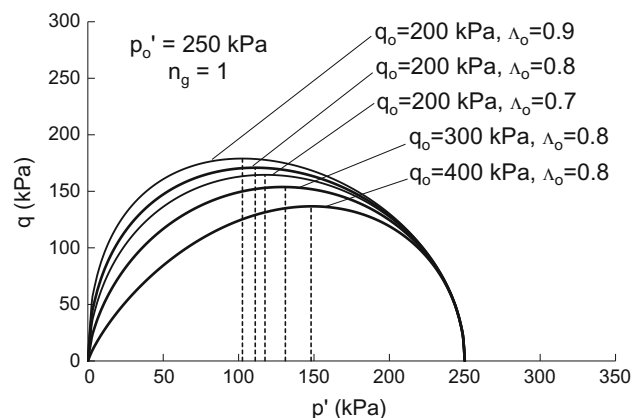

Fig. 5 Typical shapes of plastic potential surfaces in q–p' stress space, plots for $p_o' = 250$ kPa and $n_g = 1$

always remains on the current yield surface. This condition can be satisfied using the following consistency condition.

$$\dot{f} = \frac{\partial f}{\partial p'}\mathrm{d}p' + \frac{\partial f}{\partial q}\mathrm{d}q + \frac{\partial f}{\partial p'_o}\mathrm{d}p'_o + \frac{\partial f}{\partial q_o}\mathrm{d}q_o = 0 \quad (15)$$

By substituting $\mathrm{d}p_o'$ and $\mathrm{d}q_o$ from the hardening rule given in Eqs. (8) and (9), Eq. (15) can be modified to

$$\left[\frac{\partial f}{\partial p'_o}\frac{vp'_o}{(\lambda-\kappa)}\right]\mathrm{d}\varepsilon_p^{\mathrm{p}} + \left[\frac{\partial f}{\partial q_o}\frac{n_{\mathrm{f}}(1-\xi)p'^2_o}{p'_o+q_o}\psi\right]\mathrm{d}\varepsilon_q^{\mathrm{p}}$$
$$= -\left(\frac{\partial f}{\partial p'}\mathrm{d}p' + \frac{\partial f}{\partial q}\mathrm{d}q\right) \quad (16)$$

The flow rule can be defined as shown in Eq. (17).

$$\mathrm{d}\varepsilon_p^{\mathrm{p}} = \mathrm{d}\lambda\frac{\partial g}{\partial p'} \quad \text{and} \quad \mathrm{d}\varepsilon_q^{\mathrm{p}} = \mathrm{d}\lambda\frac{\partial g}{\partial q} \quad (17)$$

Using Eqs. (16) and (17), the loading function $\mathrm{d}\lambda$ can be obtained as

$$\mathrm{d}\lambda = \frac{-\left(\frac{\partial f}{\partial p'}dp' + \frac{\partial f}{\partial q}dq\right)}{n_{\mathrm{f}}(1-\xi)\dfrac{p'^2_o}{p'_o+q_o}\psi\dfrac{\partial f}{\partial q_o}\dfrac{\partial g}{\partial q} + \dfrac{vp'_o}{(\lambda-\kappa)}\dfrac{\partial f}{\partial p'_o}\dfrac{\partial g}{\partial p'}} \quad (18)$$

By substituting the derivatives $\partial f/\partial q_o$, $\partial g/\partial q$, $\partial f/\partial p_o'$ and $\partial g/\partial p'$, a general form of the incremental stress–strain relationship during elasto-plastic behavior can be written as $\mathrm{d}\varepsilon_{ij} = \mathrm{d}\varepsilon_{ij}^{\mathrm{e}} + \mathrm{d}\varepsilon_{ij}^{\mathrm{p}}$, where $d\varepsilon_{ij}^{\mathrm{e}}$ is computed using Eq. (4) and $d\varepsilon_{ij}^{\mathrm{p}}$ using Eq. (19).

$$\mathrm{d}\varepsilon_{ij}^{\mathrm{p}} = \left[\frac{1}{H}\left\langle\frac{p'}{p'^2_o}\left(1+2\ln\left(\frac{p'}{p'_o}\right)\right)\mathrm{d}p' + \frac{2q}{q^2_o}\mathrm{d}q\right\rangle\right]\frac{\partial g}{\partial \sigma_{ij}} \quad (19)$$

Here, the plastic hardening modulus H is defined as

$$H = \psi\left[\frac{4n_{\mathrm{f}}n_g(1-\xi)q^3}{q_o(p'_o+q_o)} + \frac{v}{(\lambda-\kappa)}\frac{p'^{2+R}}{p'^{1+R}_o}\Pi\right] \quad (20)$$

where, $\Pi = \left(1+2\ln\left(\frac{p'}{p'_o}\right)\right)\left(1-(R+1)\ln\left(\frac{p'_o}{p'}\right)\right)$

3 Model calibration for kaolin clay

All the model parameters can be determined from one isotropic consolidation test and a triaxial compression test on normally consolidated (NC) clay. Prashant [25] performed a series of true triaxial undrained tests and constant rate of strain (CRS) K_o consolidation tests on kaolin clay. The same data have been used to determine the model parameters for kaolin clay.

The CRS consolidation test data on kaolin clay indicated an average value of the slope of normal compression line to be $\lambda = 0.16$ and the slope of unload–reload line $\kappa = 0.018$. To use these parameters in the model, it is assumed that the slope of normal consolidation line during isotropic consolidation and K_o consolidation remains

approximately the same [40]. For the above values of λ and κ, the value of parameter $\Lambda_o = 0.89$. Lade [12] proposed an empirical relationship between plasticity index (PI) and Poisson's ratio by comparing these values for various clays. From this relationship, the Poisson's ratio for kaolin clay (PI = 32 %) can be assumed as $v = 0.28$.

The other model parameters (C_{f}, n_{f} and n_g) were calibrated by using the data from a consolidated undrained compression test on NC kaolin clay which was performed at initial effective confining pressure of $p_c' = 275$ kPa using a flexible boundary true triaxial system. The shear stress–strain relationship and pore-pressure measured during this test have been presented in Fig. 6. The peak shear strength for this test was observed to be 174 kPa. Prashant and Penumadu [28] showed that the shear strength of clay q_{f} under consolidated undrained compression test can be correlated with the initial value of mean effective stress p_i' and OCR using Eq. (21).

$$q_{\mathrm{f}} = C_{\mathrm{f}}p_i'(\mathrm{OCR})^{\Lambda_o} \quad (21)$$

Hence, the shear strength q_{fNC} of NC clay with initial value of pre-consolidation stress p_o' will be:

$$q_{\mathrm{fNC}} = C_{\mathrm{f}}p'_o \quad (22)$$

Therefore, the experimental data suggest the value of $C_{\mathrm{f}} = 0.633$. This failure strength parameter is found to be consistent with stress ratio at failure reported by Ladd and Foott [10] for normally consolidated Boston Blue clay (primarily Kaolinite) in triaxial compression.

One may note here that the Eq. (22) is valid only if the specimen reaches failure smoothly during shearing. However, the experimental observations showed a certain degree of a sudden failure response during all the tests. The soil element could have sheared to slightly higher stress state if it had not experienced sudden failure. Hence, this value of C_{f} has to be corrected considering the fact that by definition, it is applicable to smooth failure. Duncan and Chang [7] used hyperbolic relationship to define stress–strain relationship and found that it often overpredicted the strength of soil. They used a reduction factor to make correction for the strength at finite strain. Assuming the stress–strain relationship to be a hyperbolic function, Prashant and Penumadu [29] presented a rigorous way of estimating the hypothetical shear strength corresponding to no sudden failure conditions. In a simple way, a constant shear strength asymptote to the pre-peak shear stress–strain relationship can be used to estimate the actual value of q_{fNC}. Considering this value of q_{fNC} for the given NC data, Eq. (22) suggested the actual value of parameter $C_{\mathrm{f}} = 0.66$. Drawing an analogy with the work of Duncan and Chang [7], the hyperbola is used in the present model to establish an asymptote in shear stress (for reference surface), which is never actually attained by the predicted stress–strain curve. The reduction factor of [7] is
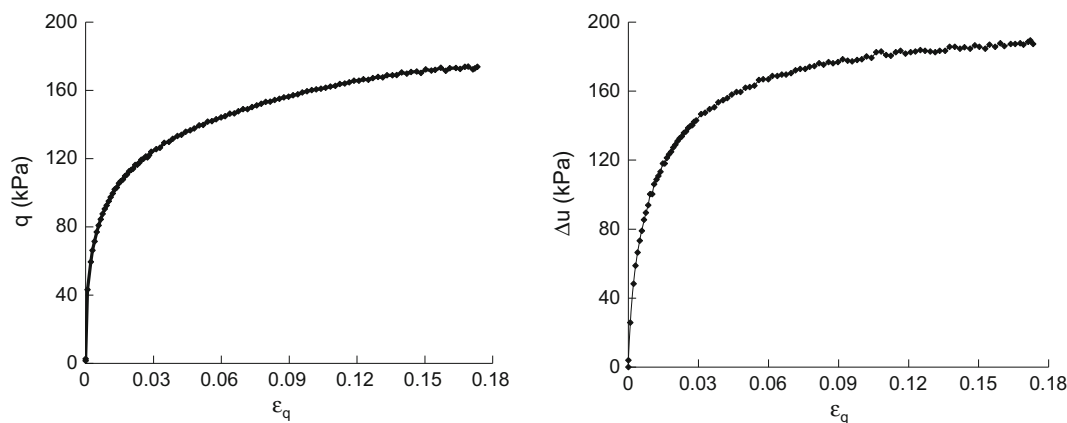
Fig. 6 Results of the isotropically consolidated true triaxial undrained compression test used to calibrate of the proposed model

analogous to asymptoting factor ψ used to simulate failure when the stress state reaches I_3 surface. Hence, the predicted response will show failure before reaching the asymptote defining the reference surface.

Hardening rule in Eq. (9) can be rewritten in incremental form as shown in Eq. (23).

$$\frac{\Delta q_o}{n_f} = (1 - \xi) \frac{p_o'^2}{p_o' + q_o} \psi \Delta \varepsilon_q^p \tag{23}$$

The values of p_o' at each point of the experimental data were calculated using Eq. (8) with known plastic volumetric deformation considering undrained condition.

Under undrained condition:

$$\Delta \varepsilon_p^p = -\Delta \varepsilon_p^e \tag{24}$$

$$\Delta \varepsilon_q^p = \Delta \varepsilon_q - \Delta \varepsilon_q^e \tag{25}$$

Elastic strain components $\Delta \varepsilon_p^e$ and $\Delta \varepsilon_q^e$ were calculated using Eqs. (2) and (4). Since the stress state will be consistently on the yield surface while it grows with the plastic deformations, the values of q_o at each point can be calculated using Eq. (5) with known values of all the other parameters in the equation. Similarly, the incremental value of the right-hand side (RHS) term in Eq. (23) can be computed with the known values of ξ and ψ from Eqs. (10) and (11), respectively. Cumulative sum of the RHS term of Eq. (23) is referred to as h_q in Eq. (26), which represents shear hardening with plastic shear strain.

$$h_q = \sum (1 - \xi) \frac{p_o'^2}{p_o' + q_o} \psi \Delta \varepsilon_q^p \tag{26}$$

Figure 7 shows the relationship between q_o and h_q, which is a reasonably linear relationship. The intercept on ordinate suggests the initial value of $q_o = 192$ kPa, and the slope of line gives the value of hardening parameter $n_f = 53$.

The flow rule given in Eq. (17) can be used to define proportionality of shear and volumetric components of
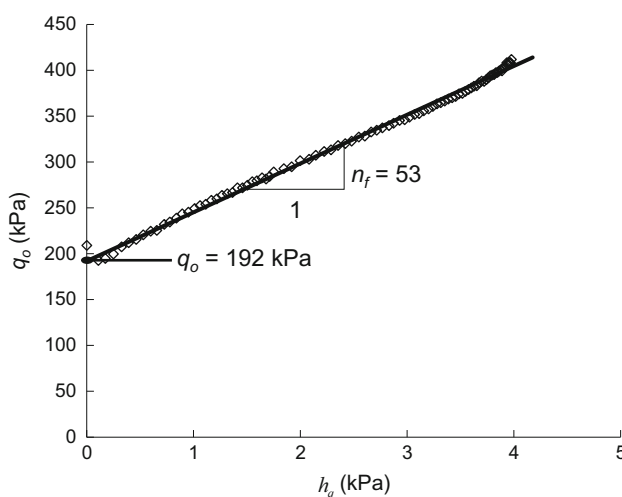

Fig. 7 Determination of hardening parameter n_f, and initial value of state variable q_o using representative shear hardening with plastic shear strain h_q

plastic strains as shown in Eq. (27). On further rearranging it using Eq. (14), one can derive shear and volumetric strain equivalents of total plastic flow as F_q in Eqs. (28) and F_p in Eq. (29), respectively.

$$\frac{d\varepsilon_q^p}{d\varepsilon_p^p} = \frac{\partial g}{\partial q} \bigg/ \frac{\partial g}{\partial p'} \tag{27}$$

$$F_q = \sum \Delta \varepsilon_q^p \frac{\partial g}{\partial p'}$$
$$= \sum \Delta \varepsilon_q^p \left[\psi p'^R p_o'^{1-R} \left(1 - (R+1) \ln \left(\frac{p_o'}{p'} \right) \right) \right] \tag{28}$$

$$F_p = \sum \frac{\Delta \varepsilon_p^p}{n_g} \frac{\partial g}{\partial q} = \sum \Delta \varepsilon_p^p \left[2q \left(\frac{q_o}{p_o'} \right)^2 \right] \tag{29}$$

The parameters involved in Eqs. (28) and (29) are the same as in Eq. (23), and their values are known at each
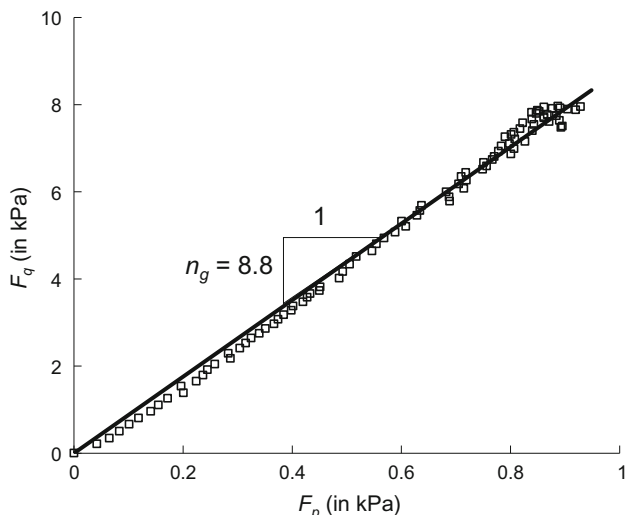
Fig. 8 Determination of plastic potential parameter n_g

Table 1 Model parameters for kaolin clay

Proposed model parameters	Value
Elastic behavior	
κ	0.018
ν	0.28
Failure surface	
C_f	0.66
Hardening parameter	
λ	0.16
n_f	53
Plastic potential	
n_g	8.8

point of the experiment. The only new parameter is R, which can also be calculated using Eq. (13) with known values of q_o and p_o' at each data point. The relationship between F_q and F_p is expected to be linear with its slope as n_g according to Eq. (27). Figure 8 shows the same relationship for NC data, which provides the value of parameter $n_g = 8.8$ for kaolin clay.

A summary of all the model parameters determined for kaolin clay is provided in Table 1. It is to be noted that q_o and p_o' are state variables. For the data used in the following section for its comparison with the model predictions, the initial value of these state variables is determined to be $q_o = 192$ kPa and $p_o' = 275$ kPa.

4 Model predictions for kaolin clay

The true triaxial undrained shear test data of [26, 27] on cubical specimens of kaolin clay were used to compare the model predictions of stress–strain and pore-pressure response for various combinations of intermediate principal stress and overconsolidation level. During these tests, the normal stress along minor principal direction σ_3 was kept constant. The major and intermediate principal stresses (σ_1 and σ_2, respectively) were increased proportionally by following a given value of intermediate principal stress ratio b defined by Eq. (30). The value of b remains the same when it is defined with respect to principal effective stresses (σ_1', σ_2', σ_3').

$$b = \frac{\sigma_2 - \sigma_3}{\sigma_1 - \sigma_3} = \frac{\sigma_2' - \sigma_3'}{\sigma_1' - \sigma_3'} \qquad (30)$$

A computer code was developed to implement the model predictions. The experiments were simulated

directly in effective stress by calculating the incremental response of a single element of material subjected to small increments in effective stress. The elastic and plastic strain increments were calculated for a given effective stress increment using Eqs. (4) and (19). The effective stress increment vector of small magnitude was rotated along a constant b value plane to satisfy the undrained condition within specified limits, i.e., the absolute value of cumulative total volumetric strain (sum of total elastic and plastic strain values) was kept within the tolerance of 10^{-8} %. The excess pore pressure was estimated from the change in mean effective stress after each step. The undrained shear behavior of a single element (of clay material) was predicted by having the initial effective stress state at hydrostatic axis and by specifying the corresponding values of three state variables v, q_o and p_o'. In the case of overconsolidated specimens, the initial effective stress state was taken inside the initial yield surface. The deformations remained elastic on loading until the effective stress state reached the current yield surface. The length of the last effective stress increment vector was adjusted to reach exactly on the initial yield surface. Further shearing caused plastic deformations, and the yield surface was updated accordingly by following the hardening rule. As the effective stress state reached close to the failure surface, the length of effective stress increment vector was reduced by many folds to capture the large shear deformations more accurately.

The true triaxial data produced by Prashant [25] included four major series of undrained shear tests on cubical specimens of kaolin clay. The first one focused on the effect of overconsolidation and included triaxial compression ($b = 0$) tests on kaolin clay specimens with OCR = 1–10. The value of OCR was defined in terms of mean effective stress. The other three series of experiments explored the effect of intermediate principal stress ($b = 0$–1) for NC, moderately OC (OCR = 5) and heavily OC (OCR = 10) kaolin clay. To simulate these experiments using the

proposed model, the soil parameters listed in Table 1 were calibrated using the data from only one of these tests, i.e., $b = 0$ shearing of NC specimen. The initial value of state variables was consistently taken as $q_o = 192$ kPa and $p_o' = 275$ kPa. The following discussion compares the predicted response to the experimental observation. The experimental data have been shown up to the peak shear stress location beyond which the sudden failure response was observed. The model assumes the post-failure shear stress and void ratio to be constant on further shearing. In reality, the clay specimens may have experienced structural changes and nonuniform deformations in the post-failure response, which will be difficult to simulate using single-element predictions. Such post-failure response is a rather complex issue and yet to be fully understood, and thus, it has been kept beyond the scope of this model.

4.1 Effect of overconsolidation

Figure 9 shows model predictions compared with the corresponding experimental data from a series of true triaxial undrained compression ($b = 0$) tests at various OCR values (OCR = 1, 1.5, 2, 5, 10). At each OCR value, the predicted stress–strain relationship, shear strength and pore-pressure response are generally in close agreement with their experimentally observed values. The test with OCR = 1 and $b = 0$ shows a relatively much better match than the other tests, which could be attributed to the fact that the model was calibrated using these test data along with the CRS test results. The effect of OCR is mainly captured through the parameter Λ_o in Eq. (21), which defines the shape of reference surface in triaxial plane. Since this parameter is a function of λ and κ values determined from one-dimensional compression test, the proposed model offers the effect of OCR to be less sensitive to model calibration.

The shear stiffness at lower strain levels was predicted well in all the cases of OCR values. The shear strength showed small deviation in case of OCR = 5. The strain at failure is nearly identical for all OCR, which is commonly observed for most of the clays. It is slightly overpredicted in most cases yet found to be reasonable. Similar to any other elasto-plasticity-based constitutive model, the proposed model shows a kink in stress–strain relationship (for OCR > 1) when the stress state intersects the initial yield surface. The predicted pore-pressure response also reflects such distinction, and especially in case of high OCR values, the pore pressure initially increases with elastic response and then reduces on subsequent plastic loading. Sometimes, transitional plasticity concepts (smooth evolution of plasticity) are used to eliminate this problem [4, 39]; however, that can complicate the formulation significantly. Striking a balance between simplicity of formulation and accuracy of results, it is perceived unnecessary to further modify the proposed model.

4.2 Effect of intermediate principal stress

The present model incorporates the effect of intermediate principal stress on stress–strain response of clay in a simplified way using an asymptoting factor with respect to the failure surface based on the third invariant of effective stress tensor. To evaluate the forte of the proposed model against the effect of intermediate principal stress on the clay behavior, the predictions were made for a series of tests at different relative magnitudes of intermediate principal stress ($b = 0.25$, 0.5, 0.75 and 1.0) using the specimens with initial OCR = 1, 5 and 10. Figures 10, 11 and 12 show comparison of the model predictions with the corresponding experimental data, which illustrate the following observations.

4.2.1 Normally consolidated kaolin clay (OCR = 1)

Figure 10 shows that the predicted shear stress–strain curves and excess pore-pressure response of NC clay compare well with the experimental observations for all the b values. The shear strength and shear strain at failure were reasonably predicted for all the cases except for the slightly underpredicted values in the case of $b = 1$. Sudden decrease in the shear stiffness was predicted near peak shear stress where the material, eventually, experienced large shear deformations. The pore pressure also became constant at the same strain where the peak shear stress occurred.

4.2.2 Moderately overconsolidated kaolin clay (OCR = 5)

The model predictions for the experiments on moderately OC clay are compared in Fig. 11. The shear stress–strain behavior followed the same curve over a reasonable range, and it was true for all the b values. The shear strength was slightly underpredicted in the case of $b \geq 0.75$; however, the predicted strain to failure indicated reasonable agreement with the experiments. Although the pore-pressure evolution in the case of $b = 0.5$ was slightly overpredicted, the predictions in other cases were within a range that could be expected due to experimental variation itself.

4.2.3 Heavily overconsolidated kaolin clay (OCR = 10)

Figure 12 shows the comparisons for heavily OC kaolin clay with different b values. The initial stiffness at lower strains was predicted well. The overall stress–strain relationship was slightly overpredicted in most cases, but a
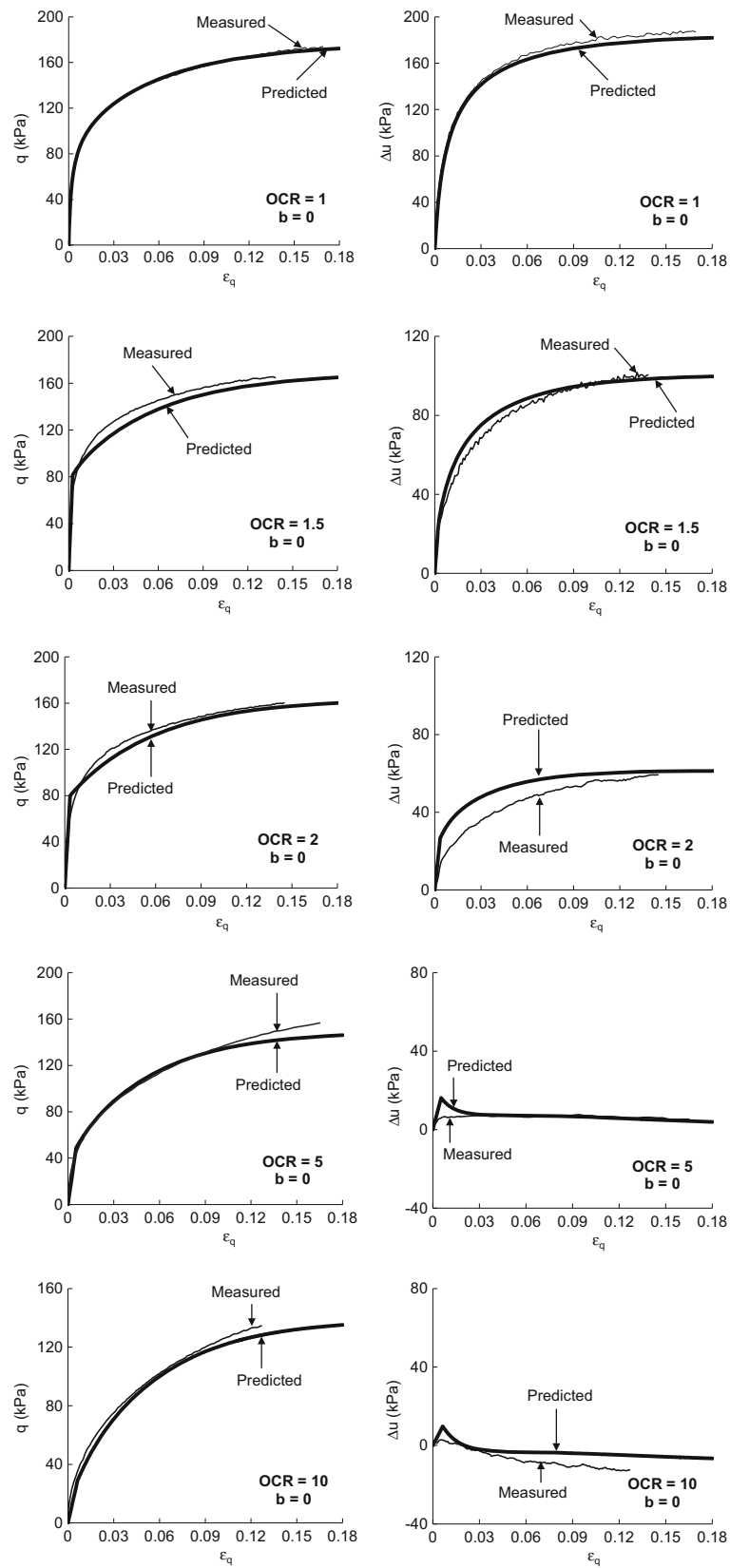
Fig. 9 Model predictions and experimental data from TT undrained compression tests ($b = 0$) on OC kaolin clay
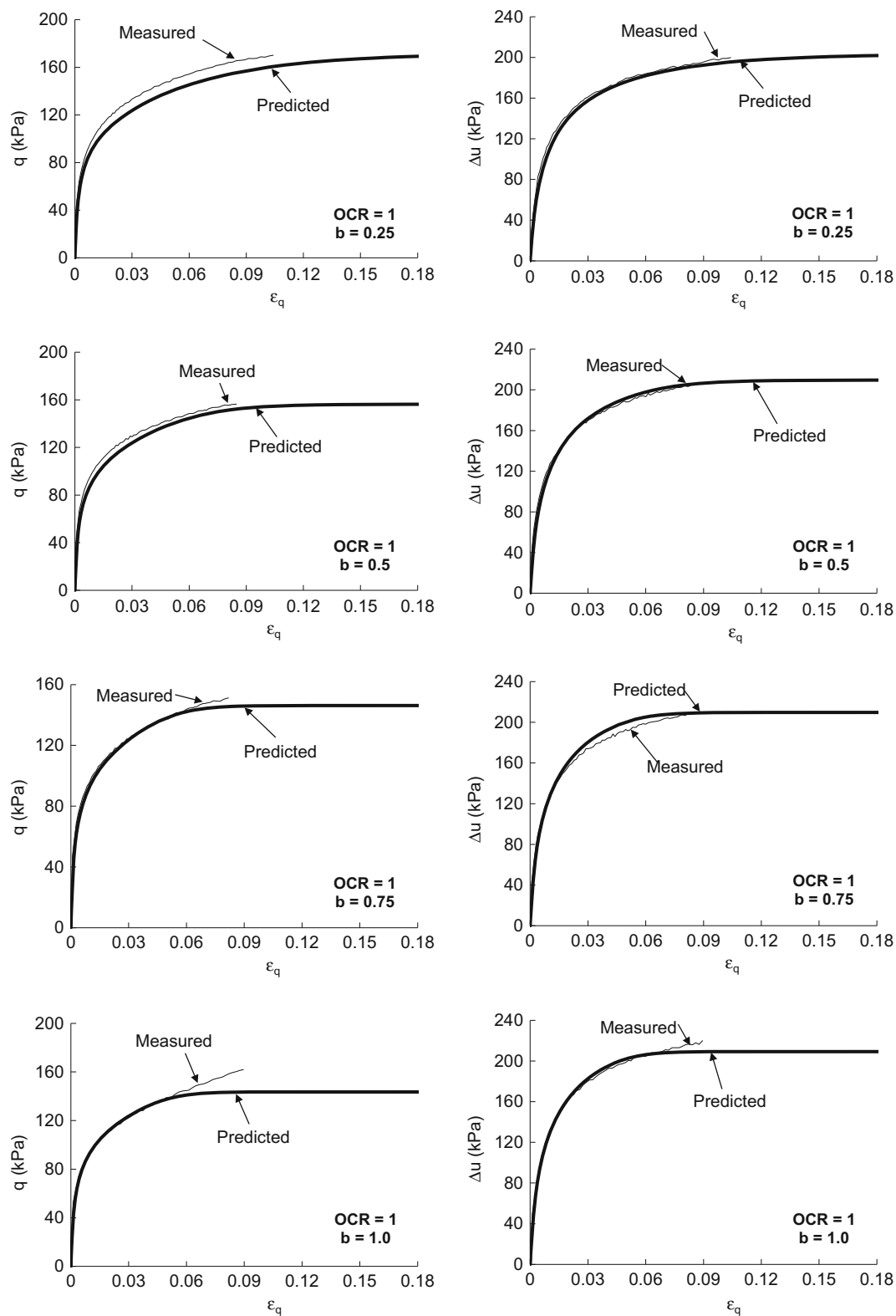
Fig. 10 Model predictions and experimental data from TT tests on NC kaolin clay

considerable variation was observed only for $b = 0.25$. The response for $b = 0$ case was also predicted well, which is shown in Fig. 9. The pore pressure was slightly overpredicted in the case of $b \geq 0.75$; however, it could be considered acceptable in view of the simplicity considered in model formulation.
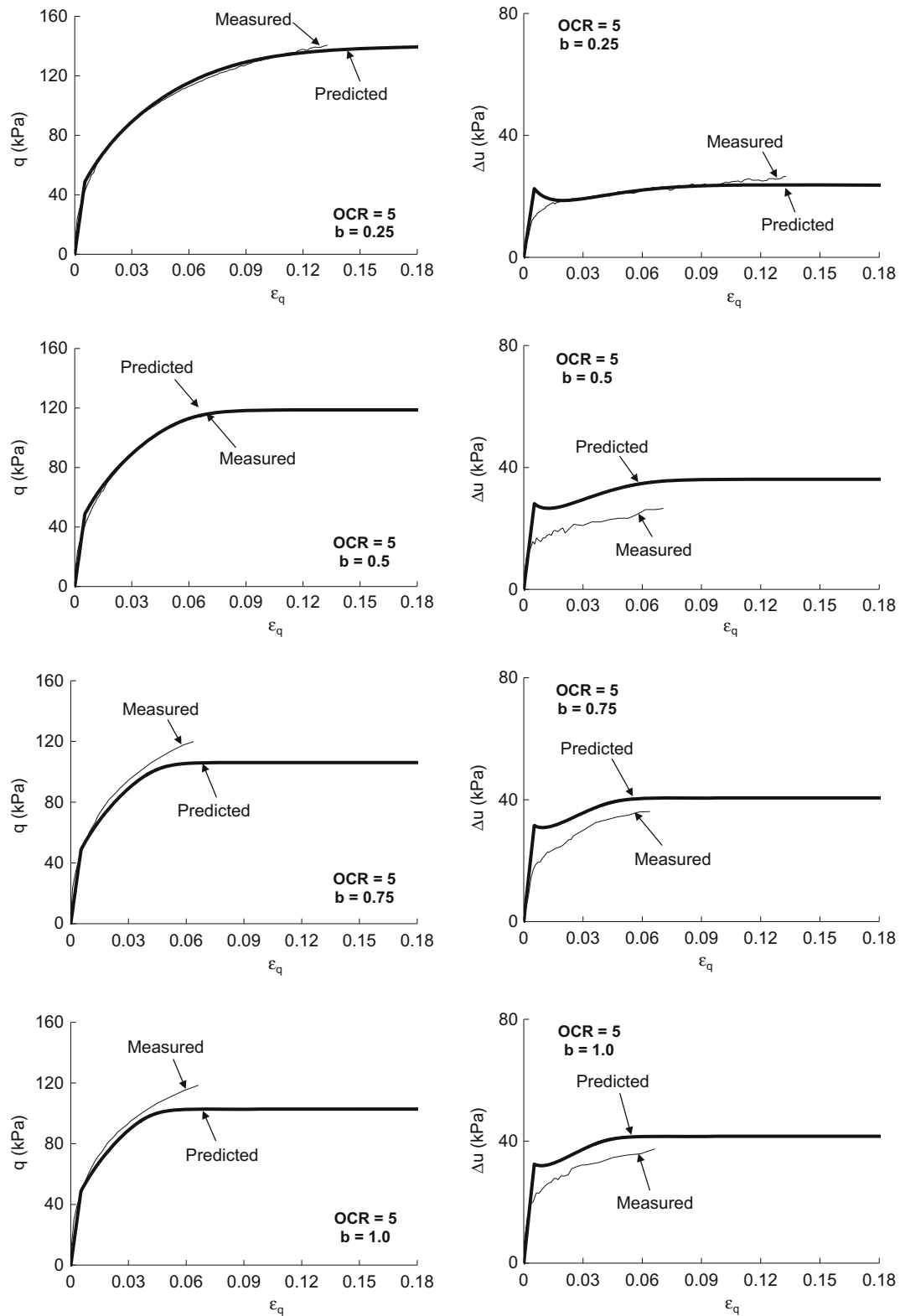
Fig. 11 Model predictions and experimental data from TT tests on OC = 5 kaolin clay

The specimens for TT experiments were prepared through one-dimensional slurry consolidation, which could induce inherent anisotropy. Prashant and Penumadu [27]

suggested that the impression of inherent anisotropy in NC specimens could be obscured; however, on unloading of the specimens to much lower confining stress, the effect of
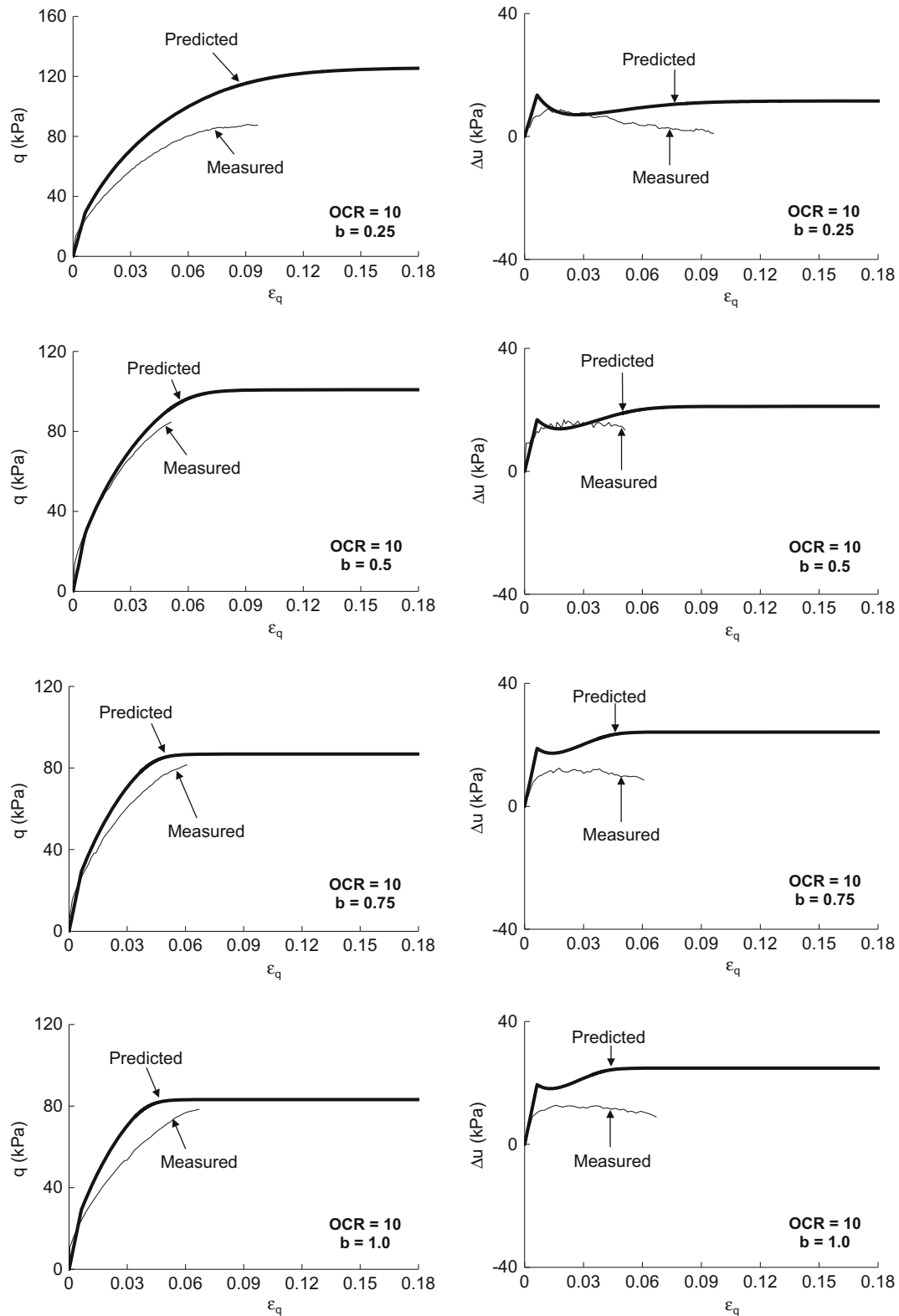
Fig. 12 Model predictions and experimental data from TT tests on OC = 10 kaolin clay

anisotropy might again become significant due to the elastic deformations contributing more significantly in the overall stress–strain response. This phenomenon explains

significant influence of the intermediate principal stress on stress–strain behavior of heavily OC clay in comparison with NC clay. This phenomenon was knowingly neglecting

during development of the proposed model to avoid complicating the formulation and increasing required number of model parameters without adding much accuracy in the predictions.

5 Summary and conclusions

A new constitutive model is proposed in this research based on the observations from an extensive experimental study on kaolin clay using true triaxial system. While the formulation has been kept with minimized complexity, the developed model is able to incorporate the complex behavior of clay including the effect of intermediate principal stress and overconsolidation. The proposed rate-independent isotropic model follows a non-associative flow rule. The shape of yield surface is defined on the basis of experimentally observed acceptable range of elastic deformation. The failure condition has been derived from the widely recognized correlation between the normalized undrained shear strength of clays and their overconsolidation level. The pre-failure plastic behavior is defined to be controlled by a reference surface, which is different from the failure surface in octahedral plane. An asymptoting factor has been introduced to model the sudden failure response in a continuous mode when the stress state reaches close to failure surface.

The six model parameters were calibrated using one each of one-dimensional compression test and triaxial compression test on kaolin clay. Using these parameters, the predicted shear stress–strain relationship and excess pore pressure both compared well with the experimental results for the effect of overconsolidation over a range of OCR values from 1 to 10. The effect of intermediate principal stress (for $b = 0, 0.25, 0.5, 0.75$ and 1.0) was predicted well for OCR = 1 and 5, and it was reasonably close to the experiments in the case of OCR = 10. The overall stress–strain relationship and shear strength were slightly underpredicted in some cases of OCR = 5 and overpredicted in some cases of OCR = 10.

References

1. Baudet B, Stallebrass S (2004) A constitutive model for structured clays. Géotechnique 54(4):269–278
2. Casey B, Germaine J (2013) Stress dependence of shear strength in fine-grained soils and correlations with liquid limit. J Geotech Geoenviron Eng 139(10):1709–1717
3. Dafalias YF (1986) Bounding surface plasticity: mathematical foundation and hypo-plasticity. J Eng Mech 112(9):966–987
4. Dafalias YF, Herrmann LR (1986) Bounding surface plasticity. II: application to isotropic cohesive soils. J Eng Mech 112(12):1263–1291
5. Dafalias YF, Manzari MT, Papadimitriou AG (2006) SANI-CLAY: simple anisotropic clay plasticity model. Int J Numer Anal Methods Geomech 30:1231–1257. doi:10.1002/nag.524
6. Drucker DC, Gibson RE, Henkel DJ (1955) Soil mechanics and work-hardening theories of plasticity. Proc ASCE 81:1–14
7. Duncan JM, Chang CY (1970) Non linear analysis of stress and strain in soils. ASCE J Soil Mech Found Div 96(SM5):1629–1653
8. Jamiolkowski M, Ladd CC, Germain JT, Lancellotta R (1985). New developments in field and laboratory testing of soils. In: Proc. of 11th Int. conf. on soil mech. and found. eng., vol 1. p 57–153
9. Jiang J, Ling HI, Kaliakin VN (2012) An associative and non-associative anisotropic bounding surface model for clay. J Appl Mech 79(3):031010
10. Ladd CC, Foott R (1974) New design procedure for stability of soft clays. J Geotech Eng Div 100(GT7):763–786
11. Lade PV (1977) Elastoplastic stress–strain theory for cohesionless soils with curved yield surface. Int J Solids Struct 13:1019–1035
12. Lade PV (1979) Stress–strain theory for normally consolidated clay. In: 3rd Int. conf. numerical methods geomechanics, Aachen, pp 1325–1337
13. Lade PV (1990) Single hardening model with application to NC clay. J Geotech Eng 116(3):394–415
14. Lade PV, Duncan JM (1975) Elastoplastic stress–strain theory for cohesionless soil. J Geotech Eng Div 101:1037–1053
15. Mašín D (2012) Hypoplastic Cam-clay model. Géotechnique 62(6):549–553
16. Mašín D (2013) Clay hypoplasticity with explicitly defined asymptotic states. Acta Geotech 8(5):481–496
17. Mašín D, Ivo H (2007) Improvement of a hypoplastic model to predict clay behaviour under undrained conditions. Acta Geotech 2(4):261–268
18. Mayne PW (1979) Discussion of "Normalized deformation parameters for kaolin" by HG. Poulos. Geotech Test J 1(2):102–106
19. Mayne PW, Swanson PG (1981) The critical-state pore pressure parameter from consolidated-undrained shear test. Lab Shear Strength Soil ASTM STP 740:410–430
20. Mroz Z (1980) Hypoelasticity and plasticity approaches to constitutive modelling of inelastic behavior of soils. Int J Numer Anal Methods Geomech 4:45–66
21. Mróz Z (1963) Non-associated flow laws in plasticity. J Méc 2:21–42
22. Oda M, Konishi J (1974) Microscopic deformation mechanism of granular material in simple shear. Soils Found 14:25–38
23. Pastor M, Zienkiewicz OC, Leung KH (1985) Simple model for transient soil loading in earthquake analysis. II. Non-associative models for sands. Int J Numer Anal Methods Geomech 9:477–498
24. Penumadu D, Skandarajah A, Chameau J-L (1998) Strain-rate effects in pressuremeter testing using a cuboidal shear device: experiments and modeling. Can Geotech J 35:27–42
25. Prashant A (2004) Three-dimensional mechanical behavior of kaolin clay with controlled microfabric using true triaxial testing. PhD Dissertation, University of Tennessee, Knoxville
26. Prashant A, Penumadu D (2004) Effect of intermediate principal stress on over-consolidated kaolin clay. J Geotech Geoenv Eng 130(3):284–292
27. Prashant A, Penumadu D (2005) Effect of overconsolidation and anisotropy of kaolin clay using true triaxial testing. Soils Found 45(3):71–82
28. Prashant A, Penumadu D (2005) On shear strength behavior of clay with sudden failure response. In: Proc. 11th IACMAG conference, Italy

29. Prevost JH (1985) A simple plasticity theory for frictional cohesionless soils. Soil Dyn Earthq Eng 4:9–17
30. Roscoe KH, Burland JB (1968) On the generalized stress–strain behavior of wet clay. In: Heyman J, Leckie FA (eds) Engineering plasticity, pp 535–609
31. Roscoe KH, Schofield AN, Wroth CP (1958) On yielding of soils. Geotechnique 8:22–53
32. Schofield AN, Wroth CP (1968) Critical state soil mechanics. McGraw-Hill, Maidenhead
33. Sultan N, Cui Y-J, Delage P (2010) Yielding and plastic behaviour of Boom clay. Géotechnique 60(9):657–666
34. Taiebat M, Dafalias YF (2010) Simple yield surface expressions appropriate for soil plasticity. Int J Geomech 10(4):161–169
35. Tatsuoka F (2007) Inelastic deformation characteristics of geomaterial. Soil stress–strain behavior: measurement, modeling and analysis. Springer, Netherlands, pp 1–108
36. Tatsuoka F, Siddiquee MSA, Park C, Sakamoto M, Abe F (1993) Modelling stress–strain relations of sand. Soils Found 33(2):60–81
37. Vardoulakis I (1988) Theoretical and experimental bounds for shear-band bifurcation strain in biaxial tests on dry sand. Res Mech 23:239–259
38. Wang Q, Lade PV (2001) Shear banding in true triaxial tests and its effect on failure in sand. J Eng Mech 127(8):754–761
39. Whittle AJ, Kavvadas MJ (1994) Formulation of MIT-E3 constitutive model for overconsolidated clays. J Geotech Eng 120(1):173–198
40. Wood DM (1990) Soil behaviour and critical state soil mechanics. Cambridge University Press, New York
41. Yao YP, Sun DA, Matsuoka H (2008) A unified constitutive model for both clay and sand with hardening parameter independent on stress path. Comput Geotech 35(2):210–222
42. Yao YP, Gao Z, Zhao J, Wan Z (2012) Modified UH model: constitutive modeling of overconsolidated clays based on a parabolic Hvorslev envelope. J Geotech Geoenv Eng 138(7):860–868
43. Yin Z, Xu Q, Hicher P (2013) A simple critical-state-based double-yield-surface model for clay behavior under complex loading. Acta Geotech 8(5):509–523
44. Zytynski M, Randolph MF, Nova R, Wroth CP (1978) On modelling the unloading–reloading behaviour of soils. Int J Numer Anal Methods Geomech 2(1):87–93